Mixing and Geometry of advected, chemically reactive scalar fields: Application to chlorine deactivation over the mid-northern latitudes

A. Wonhas

DAMTP, University of Cambridge, Cambridge, CB3 9EW, United Kingdom.

E-mail: a.wonhas@damtp.cam.ac.uk

J.C. Vassilicos

Dept. of Aeronautics, Imperial College, London, SW7 2BY, United Kingdom.

E-mail: j.c.vassilicos@ic.ac.uk

Abstract

The mixing and reaction properties of advected chemicals are determined by the fractal dimension (or Kolmogorov capacity) D' of a cut through the interface between the chemicals. We show that the amount m of reacted chemicals scales like

$$m(0) - m(\kappa) \propto \sqrt{\kappa}^{\,1-D'} \ ,$$

where κ is diffusivity of the chemicals. If interscale transfer produced by the advecting flow has a linear time dependence, then the reaction rate of chemicals scales like

$$\frac{\partial}{\partial t}\left[m(0) - m(t)\right] \propto \sqrt{t}^{\,1-3\,D'}$$

with time t. Both relations are valid in a range of times and diffusivities where the diffusive length scales of the chemicals are within the range of scales where the interface between the chemicals has a well-defined fractal dimension. We apply both relations to the problem of chlorine deactivation,

$ClO + NO_2 \rightarrow ClONO_2$, over the mid-northern latitudes. We determine numerically the Kolmogorov capacity of the interface between polar air which is comparatively rich in ClO and mid-latitude air which is comparatively rich in NO_2. Additionally, we show empirically that interscale transfer by the advecting flow can be well interpreted as having predominantly linear interscale transfer in the range of times under consideration. We can therefore explain diffusivity and time dependencies previously observed in numerical simulations. Furthermore we can extrapolate the results of such simulations down to realistically low diffusivities.

1 Introduction

Many geophysical processes in the ocean and atmosphere involve large scale advection of scalar fields. For example global circulation models are used to investigate such processes. Modelling and simulating these processes continues to be a challenge. One major difficulty is to resolve fine enough scales in order to describe the effects of small effective scalar diffusivities. Sufficient resolution is not only crucial for the understanding of mixing processes but also for the modelling of reactions between advected chemicals.

An example of such a process is chlorine deactivation over the mid-northern latitudes [20]. In a cold arctic winter, polar stratospheric clouds may form. On these clouds, heterogeneous reactions produce chlorine monoxide radicals, see [30, 11] or [15] for an overview. The chlorine activated air may subsequently get transported to the mid-northern latitudes [18] where it can catalytically deplete ozone under the influence of light. This then results in increased UV radiation over the densely populated mid-northern latitudes [31]. However chlorine may also become deactivated before it can destroy ozone. One deactivation mechanism involves the reaction between polar air, which is rich in chlorine monoxide, and mid-latitude air, which

is relatively rich in nitrogen oxides [22, 4]. It was observed in sonde [19] and aircraft [25] data that the chlorine activated air has a fine filamental structure. This filamental structure has to be resolved in order to model the deactivation process [5, 10]. However state of the art simulations cannot currently resolve such small scale structures [20, 5]. In this paper, we seek to understand how small scale scalar geometry determines the mixing and reaction process of a scalar field in order to parametrise subgrid scalar mixing and reaction.

It was shown that the geometrical properties of a scalar field determine the time and diffusivity dependence of the mixing process, at least for some special initial conditions and particular flows in a well defined range of scales and times. Examples for this relation are a fractal scalar field without advection [26, 1], a patch of scalar subject to advection by a fixed vortex [8] and a patch of scalar subject to advection by an oscillating vortex [32]. In all three cases, the scalar field interface is either fractal or spiral and its Kolmogorov capacity (or fractal dimension) [28] determines the mixing process.

In this work, we present a generalisation of these results to a much wider class of flows which allows us to explain the numerical simulation results of Tan *et al.* [20] concerning chlorine deactivation and ozone depletion over the mid-northern latitudes. The limitations of the present work are the same as those of the numerical simulations of Tan *et al.*: initial conditions are defined in terms of sharp interfaces between different chemicals, and the chemical reactions are fast and binary. Of course, we should expect general initial conditions and chemical reactions to be more involved than those considered here. However, the theory that we develop does explain the results of Tan *et al.* and should therefore serve as a springboard for the development of more comprehensive approaches in the future. The central assumption of our theory is that the flow's action results in the interface developing a multi-scale geometrical structure with a scaling well approximated by a non-

trivial Kolmogorov capacity. As well as explaining the results of Tan *et al.* [20], our approach provides a characterization of the stratospheric winds used by Tan *et al.* in terms of Kolmogorov capacities and interscale transfer properties which might be useful for future modelling of stratospheric mixing and reaction.

In section 2.1, we explain how to solve a reaction equation in terms of the solution of the equivalent non-reactive mixing problem when the chemical reaction is sufficiently fast. Then, in section 2.2, we show that if the advected scalar field has a well-defined interfacial structure with a well- defined Kolmogorov capacity, the Kolmogorov capacity determines the diffusivity scaling of the mixing process. In section 3, we study the time dependence of mixing processes. If, additionally to the Kolmogorov capacity, the interscale transfer of the flow is known to be linear or exponential, the time dependence of the mixing process can be calculated. Finally, in section 4, we apply our theory to explaining the results of the numerical experiments of Tan *et al.* [20] on chlorine deactivation over the mid-northern latitudes.

2 Diffusivity dependence of mixing and reaction processes

In this section we investigate the diffusivity κ dependence of the advection-diffusion-reaction (ADR) process of chemicals. In the specific application that we consider in section 4 this diffusivity is an effective diffusivity caused by the dynamics of horizontal advection and vertical shear (see [9]). We show that under certain circumstances, all moments m of the chemical fields fulfil

$$m(0) - m(\kappa) \propto \sqrt{\kappa}^{\,1-D'} \ . \tag{1}$$

The most important of these assumptions is that the chemical field should be characterised by well-defined interfaces such that cuts through them have a well-defined Kolmogorov capacity D'. Both fractal and spiral interfaces can have well-defined

non-trivial values of their Kolmogorov capacity. In practice, the interfaces may have a well-defined Kolmogorov capacity only in a range of scales $\epsilon_{min} \ll \epsilon \ll \epsilon_{max}$, see for example figure 1. Then the power law range of (1) is restricted to diffusivities whose corresponding diffusive length scale η is within this range. For example, the corresponding long-time diffusive length scale for a scalar field in a shear flow is given by $\eta = \sqrt{\kappa t}$, whereas for a scalar field in a strain flow with strain rate σ it is $\eta = \sqrt{\kappa \sigma^{-1}}$ (see section 2.2). The other assumptions used to obtain (1) are the following:

1. The advected chemicals are statistically isotropic and homogeneous

2. The chemicals are initially on/off scalar fields, i.e. in any small region, the chemical concentration is either approximately constant (on) or effectively zero (off).

3. The chemicals' diffusivities are sufficiently small, i.e. in the range of times under consideration, the chemicals' diffusive length-scale η is small in comparison with the overall length scale L of the problem.

4. The diffusivities of all chemicals are equal.

5. The chemicals' reactions are so fast that they are limited by the advection-diffusion process rather than by the speed of their reaction

Relation (1) is not only valid for ADR processes but also holds for advection-diffusion (AD) processes provided the moment m is replaced with the second moment of the scalar field Θ, i.e. the variance $E = \int dx\, \Theta^2$. In both, the ADR and AD cases, it is the interfacial Kolmogorov capacity which is identified as determining the diffusivity scaling. This observation proves crucial in explaining the diffusivity scalings found by Tan *et al.* in their numerical experiments on chlorine deactivation in the stratosphere. Numerical experiments with more complicated chemistry and

initial spatial distributions of chemicals would require extensions of the present approach to incorporate more detailed chemistry and various multifractal properties including concentration level dependent fractal dimensions (Kolmogorov capacities). Finally, it should be pointed out that a similar relation was effectively derived in [21] but in terms of a different fractal dimension defined in the context of chaotic advection in open flows.

Relation (1) is derived in sections 2.1 and 2.2. In section 2.1, we reduce the non-linear ADR problem to a linear AD problem. In section 2.2, we solve the AD problem by analysing the geometry of a purely advected interface and then quantifying the effect of diffusion on this interface. Assumption 1 is used in section 2.2.

2.1 Spatio-temporal chemical reactions

Overview. In this subsection we introduce the non-linear ADR system. With assumption 4, the problem decouples. Assumption 5 then gives the solution of the full non-linear problem in terms of a corresponding linear problem. Finally, assumptions 2 and 3 relate the variance of the linear solution to any moment of the full solution.

The system of reaction equations. We study one of the simplest chemical reactions, the binary reaction,

$$A + B \rightarrow C \ . \tag{2}$$

It is nevertheless not difficult to generalise the following results to more complicated reactions and systems of reactions. The reaction kinetics for well mixed chemicals which react according to (2), is described by

$$\frac{\partial}{\partial t} A(t) = -\gamma \left[A(t) \cdot B(t) \right]^{\alpha} \ , \tag{3}$$

$$\frac{\partial}{\partial t} B(t) = -\gamma \left[A(t) \cdot B(t) \right]^{\alpha} \ , \tag{4}$$

$$\frac{\partial}{\partial t}C(t) = \quad \gamma\,[A(t)\cdot B(t)]^{\alpha}\ , \tag{5}$$

where $A(t)$, $B(t)$ and $C(t)$ are the time t-dependent, non-negative chemical concentrations, γ is the reaction constant and α the order of the reaction kinetics. Allowing the chemicals to be spatially advected and diffused, the fields $A(\mathbf{x},t)$, $B(\mathbf{x},t)$ and $C(\mathbf{x},t)$ obey the following system of ADR equations

$$\frac{\partial}{\partial t}A + (\mathbf{v}\nabla)A = \kappa_A\,\nabla^2 A - \gamma\,[A\cdot B]^{\alpha}\ , \tag{6}$$

$$\frac{\partial}{\partial t}B + (\mathbf{v}\nabla)B = \kappa_B\,\nabla^2 B - \gamma\,[A\cdot B]^{\alpha}\ , \tag{7}$$

$$\frac{\partial}{\partial t}C + (\mathbf{v}\nabla)C = \kappa_C\,\nabla^2 C + \gamma\,[A\cdot B]^{\alpha}\ , \tag{8}$$

where $\mathbf{v}(\mathbf{x},t)$ is the advection velocity and κ_A, κ_B and κ_C diffusion constants of the fields A,B and C respectively.

Decoupling of the reaction equations. We consider the case wherethe diffusivities are equal for all chemicals, i.e. $\kappa_A = \kappa_B = \kappa_C = \kappa$, see assumption 4. This is a realistic assumption in the case where the diffusivity is an effective diffusivity due to a fluid dynamical mixing process [9, 20]. Then the system of coupled nonlinear partial differential equations can be partially decoupled by solving for the difference of the fields

$$f(\mathbf{x},t) = A(\mathbf{x},t) - B(\mathbf{x},t)\,. \tag{9}$$

The field f is the solution of a linear AD equation

$$\left[\frac{\partial}{\partial t} + (\mathbf{v}\nabla) - \kappa\nabla^2\right]\ f = 0\,. \tag{10}$$

With field f, the decoupled equation for field A reads

$$\left[\frac{\partial}{\partial t} + (\mathbf{v}\nabla) - \kappa\nabla^2\right]\ A = -\gamma\,[\,A\,(A-f)]^{\alpha}\ . \tag{11}$$

The equations for the other fields follow analogously. fields.

Relation between the solutions for f and for the chemical fields. Now we use assumption 5 that chemical reactions are extremely fast. The speed of the chemical

reactions is therefore limited by the diffusion of the concentration fields. We refer to this case as mixing-limited chemical reactions. It takes the time $t_d \approx \frac{\eta_c^2}{\kappa}$ for a scalar to diffuse over a length scale η_c. In comparison, the chemical reaction occurs on a time scale $t_c \approx \left(\gamma\, c_0^{2\alpha-1}\right)^{-1}$, where c_0 is the concentration of the chemicals. Both time scales are approximately equal, i.e. $t_d = t_c$, for a length scale

$$\eta_c = \sqrt{\frac{\kappa}{\gamma\, c_0^{2\alpha-1}}}\ . \tag{12}$$

If the typical scale η of the chemical filament structures is much larger than η_c, the diffusive process is much slower than the reactive process and the reaction is mixing-limited. Assume in the following a mixing-limited reaction, i.e. the reaction term in (11) is much larger than the diffusion term. The solution of (11) is then in good approximation given by

$$A(\mathbf{x},t) = f(\mathbf{x},t)\, H[f(\mathbf{x},t)]\ , \tag{13}$$

where H is the Heaviside function which is 1 for positive arguments and vanishes for all other arguments. This solution makes the non-linear reactive right hand side of (11) vanish exactly and also satisfies the left hand side of (11), except around a thin region where $f = 0$. However this region gets thinner with increasing $\frac{\gamma\, \eta^2\, c_0^{2\alpha-1}}{\kappa}$. Furthermore, the solution is stable. If a field is slightly different from solution (13), a large reaction constant will bring it almost immediately to (13). Note that (13) assumes that initial conditions $A(\mathbf{x},0)$ and $B(\mathbf{x},0)$ are not simultaneously positive at any point $\mathbf{x}$. This is a reasonable assumption because if there were regions where A and B are both initially non-zero, then the chemicals in these regions would immediately react until one of the chemicals has vanished.

Properties of f and the chemical fields. We assume that the chemical fields are initially on/off, see assumption 2. With definition (9) of f follows that f has a trinary structure, i.e. its initial values are either $+f_0$, 0 or $-f_0$. The value $+f_0$ corresponds to a region where we find chemical A and similarly, the value $-f_0$

corresponds to a region where we find chemical B. During the AD process, f maintains its trinary structure as long as assumption 3 is fulfilled, i.e. as long as the diffusive length scale η is small in comparison with the overall length scale L. Here it is assumed that the "on" amount of field A reacts completely with the "on" amount of field B. If this assumption was not fulfilled, an appropriate background field would have had to be added to f. From f's trinary structure and (13) it then follows that the chemical fields keep their on/off structure for as long as η remains much smaller than L.

Relation between the variance of f and the chemical field moments. The overall reaction of the chemicals may be measured by the chemicals total amounts or masses m, which is their first order moment, e.g.

$$m_A = \int d\mathbf{x}\; A(\mathbf{x}) \; . \tag{14}$$

From the trinary structure of field f follows that the variance, or second moment, $E = \int dx\, f^2$ of f can be related to the masses m:

$$E = f_0 \cdot (m_A + m_B) \, . \tag{15}$$

The reaction equation (2) gives

$$m_A - m_B = \text{const} \, . \tag{16}$$

This allows us to express the mass m of chemical field A in terms of the variance E of field f,

$$m_A = \frac{E}{2\, f_0} + \text{ const} \, . \tag{17}$$

Equivalent relations hold for all other moments of A because an arbitrary power n of the on/off field A is given by $A^n = f_0^{n-1} A$ and therefore all moments are related

$$\frac{1}{f_0} \int dx\; f = \frac{1}{f_0^n} \int dx\; f^n \; . \tag{18}$$

The moments of chemicals B and C follow analogously.

2.2 Diffusive properties of on/off fields

Overview. In this subsection we study the relation between geometry and the spectral properties of a field characterized by well-defined interfacial structure which is statistically homogeneous and isotropic, see assumption 1. Knowing the spectrum of such a field, we can predict its diffusivity dependence.

Geometry of interface and its relation to the spectrum. If the interface of an on/off field is isotropic, homogeneous and has a well-defined Kolmogorov capacity, the spectrum of the field is a power law $\Gamma \propto k^{-p}$ [28]. The power law exponent p is then given by the Kolmogorov capacity D' of a cut through the interface

$$D' + p = 2 \ . \tag{19}$$

The Kolmogorov capacity D' is defined by the exponent $-D'$ of the box-counting function, which gives the number of boxes of size ϵ needed to cover the cut. It is often more convenient to measure the Kolmogorov capacity D of the whole interface than the Kolmogorov capacity D' of a cut through the interface. For many fractals, among them fractals with Hausdorff dimension equal to their Kolmogorov capacity, the relation between the D' and D reads (see [6], p. 93 and references therein)

$$D - d = D' \ , \tag{20}$$

where d is the Euclidan dimension of the interface. Note that in realistic cases, the interface has a well-defined Kolmogorov capacity only in a range of scales $\epsilon_{min} \ll \epsilon \ll \epsilon_{max}$, see figure 1. Then the power law spectrum is restricted to a range of wavenumbers from $\frac{2\pi}{\epsilon_{max}}$ to $\frac{2\pi}{\epsilon_{min}}$. This means we can only apply the following theory for diffusivities whose diffusive length scale η is inside the range $\epsilon_{min} \ll \eta \ll \epsilon_{max}$.

Spectrum and diffusive properties. Diffusion smoothes out spatial structures which are much smaller than a diffusive length scale η, or equivalently, which have

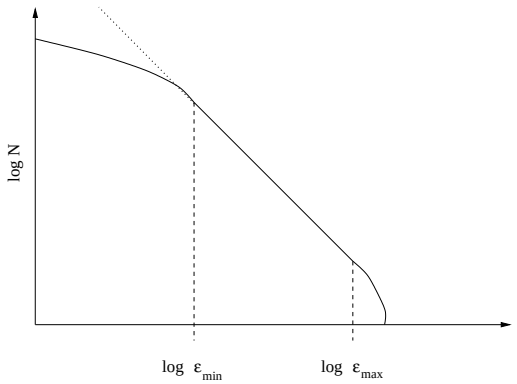

Figure 1: Schematic plot of the number N of boxes with size ϵ needed to cover an interface advected by a two-dimensional flow. Power law behaviour can be observed in a range of scales $[\epsilon_{min}, \epsilon_{max}]$. Length scales outside this range do not show power law behaviour, indicated by the dotted line. The Kolmogorov capacity D is well-defined where the box-counting function has a well-defined power law.

wavenumbers larger than a diffusive cut-off

$$k_d = \frac{2\pi}{\eta} \,. \tag{21}$$

However diffusion does not affect spatial structures which are much larger than the diffusive length scale. The diffusive length scale η depends on the type of flow, time t and diffusivity κ. For shear flows, the long-time diffusive length scale is simply the classical diffusive length scale[1]

$$\eta = \sqrt{\kappa\, t} \,. \tag{22}$$

In straining flows, the diffusive length scale becomes a constant in the long time limit

$$\eta = \sqrt{\kappa\, \sigma^{-1}} \,, \tag{23}$$

[1] In a shear flow we find two diffusive length scales: $\sqrt{\kappa\, t}$ perpendicular to the direction of shear and $\sqrt{\kappa\, t^3}$ along the direction of shear [2]. In the long time limit, the smallest structures therefore correspond to the direction perpendicular to the shear

with σ being the strain rate. Note that in both of these cases, as well as in most non-turbulent flows, the diffusive length scale has the same dependence on diffusivity, i.e. $\eta \propto \sqrt{\kappa}$. Hence the diffusive cut-off scales like $k_d \propto \kappa^{-1/2}$. Noting that the spectrum Γ is the variance per wavenumber k, the dependence of the scalar variance E on the diffusive cut-off k_d is given by

$$E(0) - E(k_d) = \int_{k_d}^{\infty} dk\, \Gamma(k) \; . \tag{24}$$

Here we have assumed a sharp diffusive cut-off, which is a good approximation as long as most of the variance has not yet diffused. Using $\Gamma(k) \propto k^{-p}$ with (19) in (24), we obtain the diffusivity dependence of the variance:

$$E(0) - E(\kappa) \propto \sqrt{\kappa}^{1-D'} \; . \tag{25}$$

This result as well as the following eq. (27) have already been obtained with less generality but higher rigour in the special cases considered in references [1, 2, 8, 26, 32].

Application. This result can now be used to predict diffusive properties of the field f, see definition (9). Assuming we know the purely advective evolution of the on-off chemical fields, we can calculate the Kolmogorov capacity D' of their interface. Then we establish the scaling of the variance of f with (25). Using (25) along with (17) and (18) we obtain relation (1) for the moments of the chemical fields A and B. From the reaction equation (2) follows $m_A(t) + m_C(t) = \text{const.}$ and hence the diffusivity dependence for the production of chemical C can also be deduced from (1):

$$m_C(\kappa) - m_C(0) \propto \sqrt{\kappa}^{1-D'} \; . \tag{26}$$

Note that we assume that the initial conditions are such that chemicals A and B neighbour each other directly. i.e. there is no gap between the fields A and B. If there was an initial gap, the results would only be applicable for diffusivities and corresponding diffusive length scales larger than the distance separating the regions

containing reactive chemicals. The theory in this section can be applied to the numerical experiments of Tan *et al.* [20] and we do so in section 4.

3 Time dependent mixing

We now predict the time-dependent mixing of a scalar field from its geometry because Tan *et al.* [20] calculated time dependencies as well as dependencies on diffusivities. If the interface of the field has a well-defined Kolmogorov capacity $0 < D' < 1$, i.e. its spectrum is a power law, we find for the rate of variance decay

$$\frac{\partial}{\partial t}\left[E(0) - E(t)\right] \propto \sqrt{t}^{\,1-3\,D'} \quad . \tag{27}$$

This result is valid if the flow reduces the size of advected scalar structures linearly with time, as is for example the case for shear flows. The result (27) is valid even if the Kolmogorov capacity D' changes with time as long as criterion (37) is fulfilled. However if a flow reduces the size of advected scalar structures exponentially with time, as is for example the case for straining flows, the rate of variance decay is given by

$$\frac{\partial}{\partial t}\left[E(0) - E(t)\right] \propto \exp[\,(1 - D')\,\sigma\,t] \;, \tag{28}$$

where σ is the average strain rate. The proportionality constants for both results are chosen such that the reaction rate becomes a continuous function. Both results are valid as long as the diffusive cut-off k_d is well within the scaling range of the spectrum. The results can readily be applied to the ADR process of chemicals by substituting the variance E with the mass m of chemicals, as described in section 2.

In section 3.1 linear as well as exponential interscale transfer are defined and ways to determine the interscale transfer of a given flow, including examples, are discussed. The derivation of result (27) for linear interscale transfer starts in section 3.2 with a description of the time-dependence of the spectrum of a fractal scalar field

undergoing linear interscale transfer. The diffusion of such a field is then calculated in cut-off diffusion approximation. Finally, if the Kolmogorov capacity varies with time, a criterion (37) is given which indicates distributions of interscale transfer rates for which (27) is applicable. The result (28) for exponential interscale transfer is given in section 3.3. Firstly, the time dependent spectrum is derived and the rate of mixing calculated. Then we discuss the case where the flow has a distribution of different exponential interscale transfer rates.

3.1 Linear and exponential interscale transfer

Definition of interscale transfer. Every scalar field can be decomposed into a superposition of waves, where each wave is characterised by its wavenumber k. The flow action generally changes the wavenumbers with time. Two distinct time dependences can be observed. First, an average linear growth in time after an initial period, i.e. $t > 1$,

$$k(t) = k(0)\, s\, t \ . \tag{29}$$

We refer to this behaviour as *linear interscale transfer*. The linear interscale transfer rate is characterised by the parameter s. Second, an average exponential growth in time, referred to as *exponential interscale transfer*, is defined by

$$k(t) \propto k(0)\ \exp(\sigma\, t)\ , \tag{30}$$

with exponential interscale transfer rate $\sigma > 0$.

Measuring interscale transfer. In most cases, it is convenient to determine the interscale transfer of a flow by measuring how the distances between pairs of tracer particles grow. Many of these pairs may separate on average either linearly or exponentially with time. The growth of separation can be directly related to the interscale transfer. Identifying point pairs as belonging to the same trough or crest of a wave, we find that neighbouring troughs or crests have to reduce their distance,

i.e. increase their wavenumber, to ensure the incompressibility of the flow. Instead of measuring point separations it is also possible to analyse the flow field derivatives. Calculating the Jacobian

$$J = \begin{pmatrix} \frac{\partial}{\partial x} v_x \, \frac{\partial}{\partial y} v_x \\ \\ \frac{\partial}{\partial x} v_y \, \frac{\partial}{\partial y} v_y \end{pmatrix} =: \begin{pmatrix} ab \\ \\ c - a \end{pmatrix} \tag{31}$$

of the 2-dimensional flow $\mathbf{v}$, we find that, locally, the flow is either a strain flow, i.e. it has two real eigenvalues, if $-\det J = a^2 + bc > 0$; a shear flow, i.e. it has one real eigenvalue, if $a^2 + bc = 0$; or a rotational flow, i.e. it has no real eigenvalue, if $a^2 + bc < 0$ (see for example [14]). Note that if velocity fields are given on discrete points, it may be too inaccurate to calculate the velocity field derivatives. In this case the method based on particle separations may be giving more reliable results.

3.2 Linear interscale transfer and mixing

Mixing by linear interscale transfer. In this subsection we consider flows with linear interscale transfer (29) and an initial power law spectrum

$$\Gamma(k) = \Gamma_0 \, (L \, k)^{-p} \ . \tag{32}$$

Our aim is to calculate how much variance ΔE is lost by diffusion in each time interval Δt. We estimate ΔE in the cut-off diffusion approximation, see section 2.2. The diffusive cut-off of a flow with linear interscale transfer is equivalent to the cut-off in a shear flow (22), i.e. $k_d = \frac{2\pi}{\sqrt{\kappa \, t}}$. To estimate ΔE, we have to determine the flux of scalar variance through the diffusive cut-off k_d in time Δt. Instead of calculating the temporal change of spectrum (32) due to interscale transfer [8], it is more convenient, in particular when describing flows with exponential interscale transfer later, to introduce an effective cut-off $k_{\rm eff}$ which represents the cut-off acting on the time-independent initial spectrum. The effective cut-off $k_{\rm eff}$ has two contributions. First, the movement of the cut-off towards smaller wave numbers due to

diffusion, i.e. $k_d \propto t^{-1/2}$ and second, the interscale transfer of variance to larger wavenumbers, i.e. $k(t) = k\,s\,t$. Both contributions result in

$$k_{\text{eff}} \propto \frac{k_d}{s\,t} \propto t^{-3/2} \; . \tag{33}$$

The change of variance ΔE due to diffusion is then simply

$$\Delta E = \Gamma(k_{\text{eff}}) \cdot \frac{\partial\, k_{\text{eff}}}{\partial\, t} \cdot \Delta t \; . \tag{34}$$

Note that k_{eff} depends on the interscale transfer rate s. Generally, different regions of the flow may have different interscale transfer rates s. Hence we introduce a probability distribution function of interscale transfer rates $P(s)$, resulting in a change of variance

$$\Delta E = -\Gamma_0 \int ds\; P(s) \left(\frac{L\,\frac{2\pi}{\sqrt{\kappa t}}}{s\,t} \right)^{-p} \cdot \frac{3\pi}{s\,\sqrt{\kappa}}\, t^{-5/2} \cdot \Delta t \; . \tag{35}$$

Expressing the spectral exponent with the Kolmogorov capacity, see (19), the time-scaling of the variance decay (27) follows in the limit $\Delta t \to 0$.

Role of changing dimensions. In some flows, in particular the one studied in section 4, the Kolmogorov capacity, and therefore the exponent of the scalar spectrum, may change with time. A flow with pure linear interscale transfer has a constant Kolmogorov capacity. However in some flows, linear interscale transfer may account for most of the scalar interscale transfer but a few flow regions may have a different interscale transfer and cause a time dependent spectral slope $p(t)$. In this case, the change in scalar variance (35) has an additional time dependent term

$$g[p(t)] = \int ds\; P(s)\; s^{\,p(t)-1} \; . \tag{36}$$

This term depends on the distribution of interscale transfer rates and the variation of the spectral slope. Generally, the broader the distribution of transfer rates, the larger the influence of this term. However as long as the relative influence of this term is small, result (27) is also valid for time dependent Kolmogorov capacities.

The influence of this term can be estimated with the minimal p_{min} and maximal p_{max} values of $p(t)$. The term is negligible if its relative variation is small, i.e.

$$\frac{|g(p_{min}) - g(p_{max})|}{\min[g(p_{max}), g(p_{min})]} \ll 1 \,. \tag{37}$$

3.3 Exponential interscale transfer and mixing

Mixing by exponential interscale transfer. In this section we assume a flow with exponential interscale transfer, again advecting a scalar field with initial power law scalar spectrum (32). Following the arguments in the previous section 3.2, we calculate the change of scalar variance ΔE per time interval Δt in the cut-off diffusion approximation. In the case of exponential interscale transfer, there is only one time-dependent contribution to the effective cut-off k_{eff} because the diffusive cut-off becomes time-independent $k_d = 2\pi\sqrt{\frac{\sigma}{\kappa}}$, see (23). Therefore the only time-dependent contribution to k_{eff} is the interscale transfer term (30), i.e.

$$k_{\text{eff}} = k_d \, \exp(-\sigma\, t) \,. \tag{38}$$

The change of variance ΔE is then obtained with (34),

$$\Delta E = -\Gamma_0 \left(\frac{2\pi\, L \sqrt{\frac{\sigma}{\kappa}}}{\exp(\sigma\, t)} \right)^{-p} \cdot 2\pi\, \sigma \sqrt{\frac{\sigma}{\kappa}} \exp(-\sigma\, t) \cdot \Delta t \,, \tag{39}$$

which gives (28). In contrast to the case with linear interscale transfer, the exponential interscale transfer causes a much faster rate of decay. Obviously result (28) is only valid for times when a significant part of the spectrum has not yet decayed. If the interscale transfer has transported most of the spectrum to wavenumbers beyond the diffusive cut-off, a different mechanism of decay sets in [7, 33].

Distribution of interscale transfer rates. For many flows, different flow regions may have different rates of interscale transfer. We can generalise our result in these cases by introducing the distribution of exponential interscale transfer rates $P(\sigma)$, which is equivalent to the introduction of the distribution of linear interscale transfer

rates in section 3.2. Then we find for the rate of variance decay

$$\frac{\partial}{\partial t}\,[E(0)-E(t)] \propto \int d\sigma\; P(\sigma)\; \exp[\,(1-D')\,\sigma\,t] \;. \tag{40}$$

Depending on the distribution of interscale transfer rates, the rate of variance decay is a superposition of exponentials with different rates of decay. In contrast to the case with linear interscale transfer, no simpler dependence on time for the rate of variance decay can be derived. In the linear case we were able to generalise the result because the interscale transfer rates appeared as factors.

4 Chlorine deactivation in the mid-northern latitudes

4.1 Diffusivity dependence of chlorine deactivation

Previous results. The theory developed in sections 2 and 3 can now be used to explain the deactivation of chlorine in mid-northern latitudes, i.e. 30°N to 60°N, in the numerical experiments of Tan *et al.*[20] . Tan *et al.* have studied a deactivation process [22, 4] where ClO mixes with mid-northern latitude air, which is rich in nitrogen oxides NO_x, and therefore deactivates[2] to chlorine nitrate

$$ClO + NO_2 \rightarrow ClONO_2 \;. \tag{41}$$

They observed, in situations where the diffusivities are as close as possible to the realistic diffusivities, that the produced amount of chlorine nitrate has a power law dependence on the effective diffusivity of the chemicals:

$$m_{ClONO_2}(\kappa) \propto \kappa^{\beta} \;. \tag{42}$$

[2]When the ClO gets bound in $ClONO_2$ it cannot deplete ozone anymore. However if the $ClONO_2$ gets broken up again by some mechanism and sets free chlorine radicals, it can indirectly cause ozone depletion.

Day	β	Range of diffusivities κ in $\mathrm{m^2 s^{-1}}$
3	0.60	$2.88 \times 10^4 \ldots 6.68 \times 10^7$
7	0.45	$2.88 \times 10^4 \ldots 4.12 \times 10^6$
11	0.30	$2.88 \times 10^4 \ldots 4.12 \times 10^6$

Table 1: Exponent β of the dependence of $ClONO_2$ production (42) on the diffusivity κ for different days. Each exponent was measured in the given range of diffusivities. Values are taken from Tan et al. [20].

They used an initial condition called Axisymm–090192, where the ClO rich air is north of 60°N and the NO_2 rich air is south of 55°N. For scalar advection on the 475 K isentrope, which is approximately at 20 km altitude, Tan et al. started their simulation on 9 January 1992 and observed after 3, 7 and 11 days the exponents β as given in table 1, see their figure 7.

Limitations of direct simulations. The numerical simulation of the ADR process by Tan et al. employed effective diffusivities which were only as low as $\kappa = 2.88 \times 10^4$ $\mathrm{m^2 s^{-1}}$, whereas realistic effective diffusivities are somewhere between 6×10^0 $\mathrm{m^2 s^{-1}}$ and 1.25×10^4 $\mathrm{m^2 s^{-1}}$ with $\kappa = 10^3$ $\mathrm{m^2 s^{-1}}$ being a more credible upper limit [20, 29]. The lower the diffusivity, the finer the structures that have to be resolved. However it is currently computationally extremely expensive to resolve the length scales of a few kilometers which would be required to simulate realistically low diffusivities. State of the art simulations can only resolve structures of a few hundred kilometers [20, 5]. Nevertheless, this deactivation process depends crucially on resolving the fine scale structures [5, 10]. The simulation by Tan et al. gives therefore only an upper bound to the production of chlorine nitrate. The approach presented here firstly confirms and explains the power law observed by Tan et al. in terms of the Kolmogorov capacity of the chemicals and, secondly, extends its validity to realistic values of the diffusivity.

Applicability of our theory. The ClO deactivation reaction (41) is a binary reaction like (2). For the relation (26) between the production of chemical C, in this case chlorine nitrate, and the geometry of the advected field to be valid, we have to verify that all chemicals have the same diffusivities, that all concentration fields are initially on/off fields and that the reaction is mixing limited. Analysing the model of Tan et al. [20], we find that all these conditions are fulfilled. The diffusivity of chemicals in an isentropic layer of the stratosphere is identical for all different chemical species because it is an effective diffusivity caused by the dynamics of horizontal advection and vertical shear [9]. The fields' initial condition has on/off character. Finally, the chemical reactions are mixing limited. The width of filaments for diffusivities as low as $\kappa = 10^3$ m^{2}s^{-1} is $\eta = 20 \times 10^3$ m [20]. This length-scale is an order of magnitude larger than the scale $\eta_c = 10^3$ m, which follows with $c_0 = 10^9$ cm^{-3}molec and $\gamma = 10^{-12}$ cm^{3}molec^{-1}s^{-1} from (12). Hence reactions are mixing limited because $\eta \gg \eta_c$.

Simulation. To predict the diffusivity scaling of the total mass (26), the Kolmogorov capacity of the advected scalar interface has to be calculated. We carry out a two-dimensional contour advection simulation which is a good approximation of the atmospheric processes because of the stable stratification of the stratosphere. The scalar interface is represented by a point set which preserves the continuity of the filament. The advection algorithm increases the number of points representing the interface to compensate for the interface stretching. The advection of each interface point uses a second order accurate Runge-Kutta integration. The interface is advected by divergence free winds from the European Centre for Medium-Range Weather Forecasts which were interpolated to the 475 K isentrope. The dataset starts on 9 January 1992 and ends on 24 January 1992 (we have also used another dataset for some checks which starts on 1 January 1995 and ends on 16 January 1995). The winds are defined on a grid with longitudinal and latitudinal resolu-

tion of about 4°. The temporal resolution is 6 hours. Between grid points and time slices, the winds are interpolated linearly. The temporal and spatial resolution of the wind-field suggests that interfaces of filaments as small as 70 km are correctly positioned [12]. The relative positioning of interfaces is presumably even less sensitive to the resolution of the wind-field. Therefore we expect the Kolmogorov capacities derived from advection by this large-scale wind-field to be accurate.

Results of advection process. Our initial interface lies at 60°N, see figure 2 day 0, corresponding to ClO rich air north of 60°N and NO_2 rich air south of this latitude. We have chosen this particular initial condition because it is close to the Axisymm-090192 initial condition of Tan et al. [20] and therefore allows us to compare our results with theirs. Note that the small initial gap of 5° or 550 km between ClO and NO_2 rich air in the simulation of Tan et al. is not important for the results of our simulation. Consider firstly that this length scale decreases quickly during the advection process and secondly that the diffusive length scale is in the order of magnitude of 100 km. Figure 2 shows the advected interface at days 0, 3, 7, 11 and 15. We observe the production of more and more small scale curl and fold structures with time. These structures give rise to a non-trivial Kolmogorov capacity.

Box counting analysis. We use a box-counting algorithm to determine the Kolmogorov capacity of the interface. Standard box-counting algorithms divide the embedding space of the interface into equally sized boxes and count the number of boxes needed to cover the interface. However it is impossible to cover a sphere with equally sized squares. Therefore a special covering of the sphere had to be employed. First, a spiral with equally spaced arms is constructed on the sphere. It is only in a small region around the pole which has the size of the arm spacing where the spacing is not well-defined. The spiral reads with longitude λ and latitude φ

$$\lambda = x \bmod 2\pi \; ; \tag{43}$$

$$\varphi = \frac{\pi}{2} - \frac{\epsilon}{2\pi R}\, x \; , \tag{44}$$

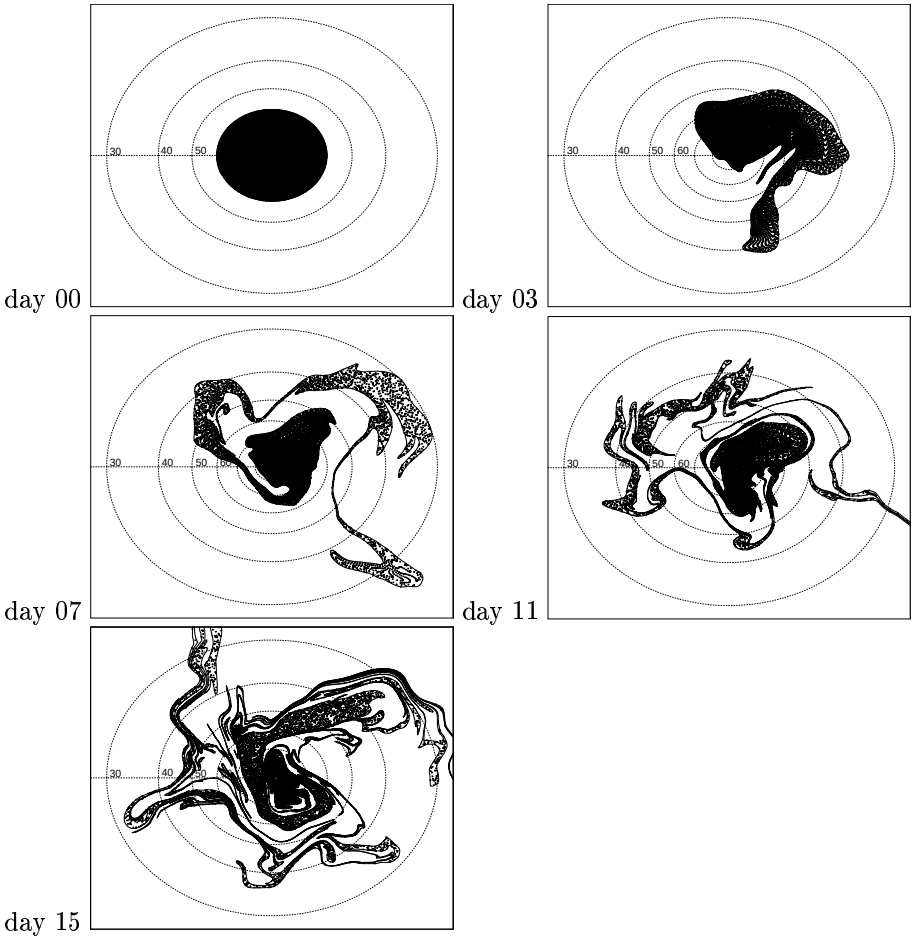

Figure 2: Stereographic projections of an interface and 10^5 tracer particles on different days. The graphs are obtained by a two-dimensional contour advection simulation which is based on measured stratospheric winds on the 475 K isentrope. The interface is given by a solid line, the tracer particles as points. Latitudes are depicted by dotted lines in 10° intervals, with latitudes 30°N to 60°N indicated by numerals 30 to 60. Initially, on 9 January 1992, the interface was aligned with the $\phi = 60^\circ$N latitude. With time, more and more curl and fold structures are produced which give rise to a non-trivial Kolmogorov capacity.

where ϵ is the distance between spiral arms, R the radius of the sphere and x the parametrisation of the spiral. The length L of the spiral can be expressed in terms of its parametrisation x:

$$L(x) = \frac{2\pi R^2}{\epsilon}\left[1 - \cos\left(\frac{\epsilon}{2\pi R}x\right)\right] \ . \tag{45}$$

Second, boxes are defined by the spiral arms and orthogonal cuts of the spiral at equal distances ϵ. Then it is easy to number all boxes, beginning from the centre. Calculating the parameter

$$x_0 = 2\pi\,\mathrm{INT}\left[\frac{R}{\epsilon}\left(\frac{\pi}{2} - \varphi\right)\right] + \lambda \tag{46}$$

corresponding to a point (λ, φ), the number n of its surrounding box is given by

$$n = \mathrm{INT}\left[\frac{L(x_0)}{\epsilon}\right] \ . \tag{47}$$

An algorithm based on spiral coverings of the sphere proved to be faster and less memory intensive than a standard box-counting algorithm based on embedding the sphere in a 3-dimensional space and applying the box-counting to this embedding space. The box-counting analysis here is carried out over the interface in the mid-northern latitudes 30°N to 60°N because we are interested in the reaction rates in this region.

Results of box-counting. The results of the box-counting after each day of advection are given in figure 3. We observe that on all days, the box-counting curves are not too far from linear, which implies that power law behaviour on intermediate scales might well approximate the box-counting functions. The power law exponents of the box-counting functions define the Kolmogorov capacities of the interface for different days. It is known that ozone distributions in the atmosphere do indeed show fractal properties, for example measured by Hurst exponents [23, 24].

Measurements of Kolmogorov capacities. In order to analyse the power law behaviour of the box-counting $N(\epsilon)$ in more detail, we have used an algorithm [27]

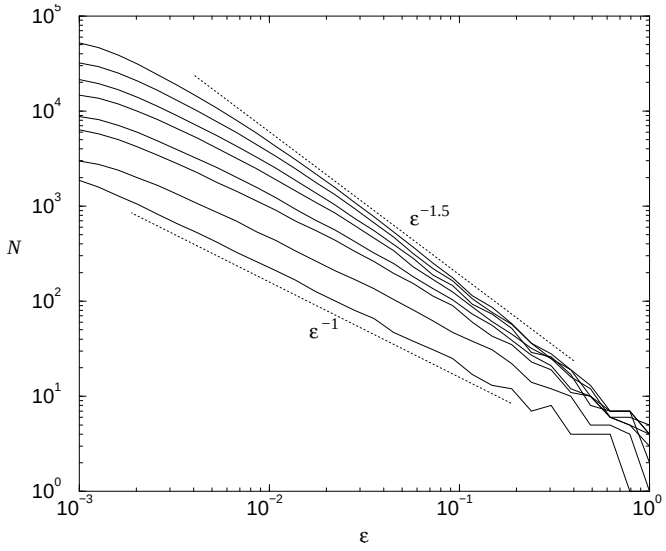

Figure 3: Time-evolution of the interface box-counting function. The abscissa of the logarithmic plot gives the length scale ϵ as fraction of the earth's radius. The ordinate denotes the number of boxes N needed to cover the interface. The curves are box-counting analyses carried out on all odd days 1,3,5,...,15. The lower a curve, the shorter was the corresponding advection of the interface. All interfaces can be reasonably well fit with a power law for intermediate scales. The power law exponent increases with time. Power laws corresponding to Kolmogorov capacities 1 and 1.5 are depicted by dotted lines.

that automatically detects the exponent and scaling range that best fits a given $N(\epsilon)$. The algorithm also provides a measure for the quality of the power law in terms of the standard deviation of possible exponent distributions. The results of this analysis are given in figure 4. These results suggest that, for the intents and purposes of this application, Kolmogorov capacities can be assigned to the box-counting functions in a range of scales from (on average) $\epsilon_{min} = 4 \times 10^{-3} R_e$ to $\epsilon_{max} = 1 \times 10^{-1} R_e$, where $R_e = 6370$ km is the earth's radius. Both length scales can be translated into diffusivities κ using the minimal diffusive length scale $\sqrt{\kappa\sigma^{-1}}$ in a flow with average strain rate σ, which can be measured to be $\sigma = 0.25$ d^{-1} by analysing the growth of the length of the advected interface [16], see figure 7. The resulting diffusivities are $\kappa = 2\times10^3$ m^{2}s^{-1} and $\kappa = 1\times10^6$m^{2}s^{-1}. Both diffusivities give respectively the lower and upper bound of the applicability of our theory and specifically (26). The lower bound is a realistic value for effective diffusion in the stratosphere. We also observe that on the first three days, the interface has a Kolmogorov capacity $D = 1$, i.e. it is a line like object. However after day 3, the Kolmogorov capacity increases about linearly with time to reach about $D = 1.5$ on day 15. For longer times, we expect that the Kolmogorov capacity eventually becomes a constant, which may be 2, the value corresponding to a space-filling interface. All in all, our box-counting analysis reveals that, on intermediate length and time scales relevant to our problem, a first approximation scaling behaviour can be observed. Using this first approximation results of our box-counting analysis and relation (26), we are now in a position to predict how the reaction rate depends on diffusivity κ.

Comparison with previous results. For days 7 and 11, the days Tan et al. have investigated, we find Kolmogorov capacities of $D = 1.14\pm0.06$ and $D = 1.32\pm0.08$, respectively. With (26), the diffusivity dependence of $ClONO_2$ production (42) is given by $\beta = 0.43 \pm 0.03$ and $\beta = 0.34 \pm 0.04$, respectively. This is in agreement

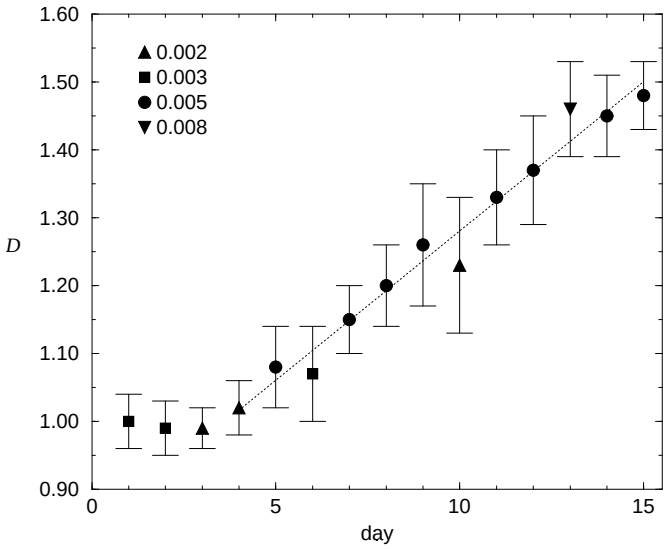

Figure 4: Kolmogorov capacities of the advected interface on different days. The Kolmogorov capacities are obtained with an algorithm [27] that automatically detects the exponent and scaling range best fitting a given box-counting function. The upper limit of the scaling range is $\epsilon_{max} = 0.1R_e$ and the lower limits ϵ_{min} detected by the algorithm are given at the upper left corner of the plot in units of 1 R_e. Error bars correspond to standard deviations of possible fit exponent distributions. The dotted line denotes a linear interpolation of the growth of the dimension with time between days 3 to 15. The Kolmogorov capacities together with 26) allow us to predict how the reaction rate depends on the diffusivity.

with the results by Tan et al. who found $\beta = 0.45$ and $\beta = 0.30$, respectively. Note that our theory cannot be applied on day 3, which was also investigated by Tan et al. Generally, our theory is restricted to days when the interface has developed a non trivial Kolmogorov capacity. On day 3, the Kolmogorov capacity is almost identical to its topological dimension. Furthermore the prediction breaks down for diffusivities larger than 1×10^6 m^{2}s^{-1}, because for larger diffusivities, the corresponding length scales are outside the scaling region of the box-counting function. Hence in this region no well-defined power law for the spectrum exists.

Extension of previous results. Not only do our results agree with Tan et al., they also extend the power law for the reaction rates to realistic diffusivities, which were previously not accessible to numerical simulations. Our results show that the power laws extend to diffusivities as low as $\kappa = 2 \times 10^3$ m^{2}s^{-1}. Additionally it is possible to predict power laws for even longer advection periods than previously investigated. For example after 15 days, the interface has a Kolmogorov capacity of $D = 1.48 \pm 0.05$, which means we expect the total amount of $ClONO_2$ to depend on the diffusivity κ like $\kappa^{0.26 \pm 0.03}$.

Rates of ozone depletion. It is also possible to apply our results to the calculation of the rate of ozone depletion. Assuming that ozone never depletes completely, the Molina cycle [13] leads to the rate of ozone depletion being proportional to the square of the ClO concentration. Because we consider effectively on/off fields, the square of the ClO concentration is proportional to the ClO mass, see (18). Therefore the rate of ozone depletion $r = \partial c_{O_3}/\partial t$, where c_{O_3} is the ozone concentration, obeys a power law equivalent to (1): $r(0) - r(\kappa) \propto \sqrt{\kappa}^{1-D'}$. This diffusivity dependence is again valid for diffusivities $\kappa = 2 \times 10^3$ m^{2}s^{-1} to $\kappa = 1 \times 10^6$m^{2}s^{-1}. Figure 5 shows the predicted rates of ozone depletion and compares them with results by Tan et al. In contrast to the full simulation of an ADR process, the simple tracking of the interface evolution and subsequent box-counting analysis is numerically much

cheaper. The current numerical analysis takes less than one hour on a standard workstation.

4.2 Time dependence of chlorine deactivation

Measurement of interscale transfer. In section 3 we have developed a method to predict the chemical reaction rate dependence on time. In order to apply our results, we have to establish the interscale transfer properties of the wind field. We measure interscale transfer by tracking the separation of tracer particle pairs in the vicinity of the interface. We observe for winds measured on the 475 K isentrope in two periods (from 09/01/92 to 24/01/92 and 01/01/95 to 16/01/95) that particle pairs separate linearly both on average and typically. This result does not seem to depend critically on the initial positions of the particles within the polar and mid-latitude regions. Figure 6a shows the linearly growing average separation between particle pairs in the vicinity of the interface. Following individual pairs, we observe that most pairs separate slowly; only a few pairs seem to separate much faster. In order to investigate the behaviour of individual particle pairs in detail, we have calculated linear and exponential fits to each particle pair separation. The quality of each fit is assessed by calculating $\mathrm{err} = \sqrt{1/N \sum_i (s_i - f_i)^2}$, where s_i and f_i are respectively the separation and the fit to the separations at time step $i = 1, \ldots, N$. The histogram in figure 6b shows the ratio of errors for the linear and the exponential fits. We observe that 46% of all trajectories are better fitted by a linear rather than by an exponential growth. For most of the remaining trajectories, the linear fit is only slightly worse than the exponential fit, suggesting that the particle separation is still well approximated by a linear function. The linear particle pair separation, both on average and typically, can be explained by assuming that on the time scales under consideration most of the flow behaves like a shear flow with the exception of only a few isolated straining or chaotic regions which cause fast exponential

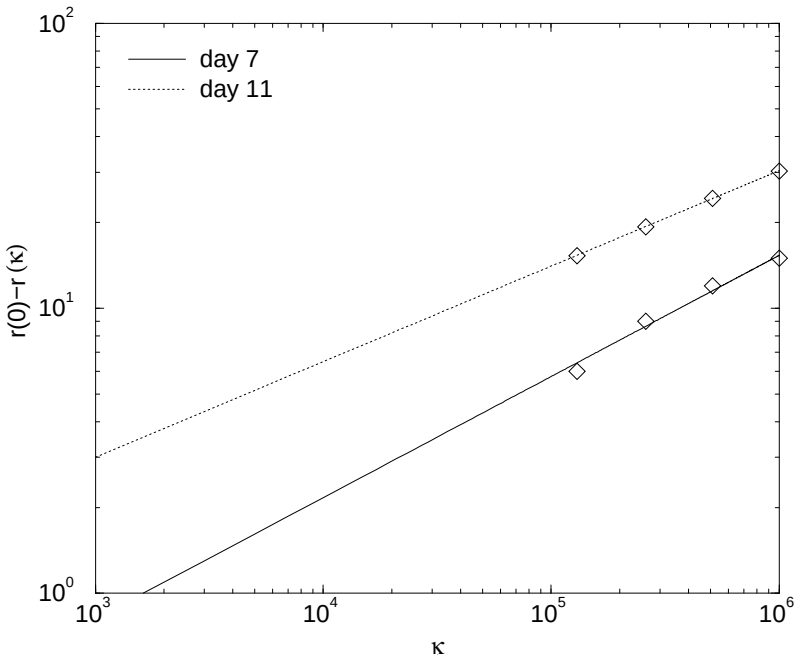

Figure 5: Diffusivity κ [m^2 s^{-1}] dependence of the rate of ozone depletion $r(\kappa)$ [ppbv/d] for selected days. The scaling of $r(0) - r(\kappa)$ is calculated with (1) and the fractal dimensions from figure 4. Diamonds represent results [20] which were obtained by a numerical solution of (6) to (8). We observe that for increasing time, the diffusivity dependence becomes shallower due to the increased dimension of the chemicals' interface. The multiplicative constant of the power law is chosen to fit the results [20] for an initial ClO concentration of 2 ppbv and an initial NO_2 concentration of 0.6 ppbv.

separation. This picture of linear particle separation may seem to contradict the exponential growth of the whole interface, see figure 7, and the common belief that advection in the stratosphere has chaotic character [17, 3], i.e. exponential particle pair separation. The exponential growth of the interface can in principle be explained by the existence of only a few straining or chaotic regions in the flow. The exponential growth in these regions is sufficient to inundate the linear growth of most of the interface in the remaining regions. It would be useful to carry out a more detailed study of particle pair separation in the stratosphere to confirm this view. It is certainly not sufficient to measure finite time "Lyapunov exponents" by fitting exponentials to the observed separation trajectories because using such a standard algorithm, we observe distributions of finite time "Lyapunov exponents", see figure 8, which are comparable to existing results [17] although we know, at least in our case, that particle pairs may equally well be interpreted to be separating linearly both on average and typically. Note however that on time scales longer than the ones considered here, particle pairs may well separate exponentially. For example if, for long enough times, the straining or chaotic regions visit all regions of the flow and, furthermore, if particle pairs remain in these regions for a time sufficiently long to align themselves with the main straining direction, the average long time particle separation would be exponential.

In summary, here we take the view that particle pairs in the vicinity of the interface separate linearly both on average and typically on the time scales relevant to our problem. Therefore we assume that the flow has dominantly linear interscale transfer and we show that the consequence of this assumption for the time dependence of reaction rates agrees with other numerical observations.

Time dependent mixing properties. Having established that the stratospheric wind field can be interpreted as having predominantly linear interscale transfer on the time-scales under consideration, we can predict the rate of $ClONO_2$ production

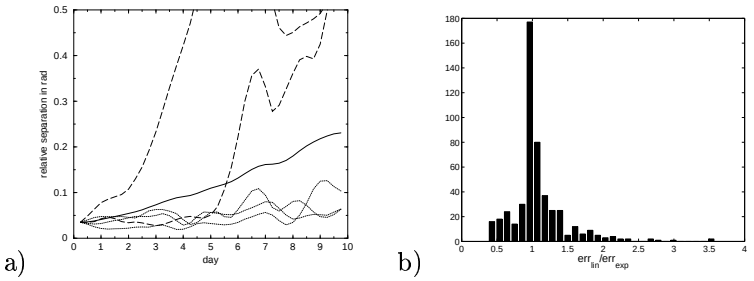

Figure 6: a) Growth of two-particle separations in radians for advection by a stratospheric wind field. Solid line: average growth of the separation between 500 tracer particle pairs; Dotted/dashed lines: Growth of the separation of selected tracer particle pairs. We observe that most particle pairs seem to separate linearly both on average (solid line) and typically (dotted lines). Only a few particle pairs separate suddenly exponentially (dashed lines). b) Histogram of the ratio of the error of a linear fit err_{lin} to the particle separation and the error of an exponential fit err_{exp} to the particle separation. The separation of 46% of particle pairs is better described by a linear fit than by an exponential fit. The separation behaviour of most remaining particle pairs is still well approximated by a linear fit. Initially, the tracer pairs for both figures were in a narrow band around the initial interface, i.e. between latitudes 58°N and 62°N. The initial separation between two particles of a pair was 2°.

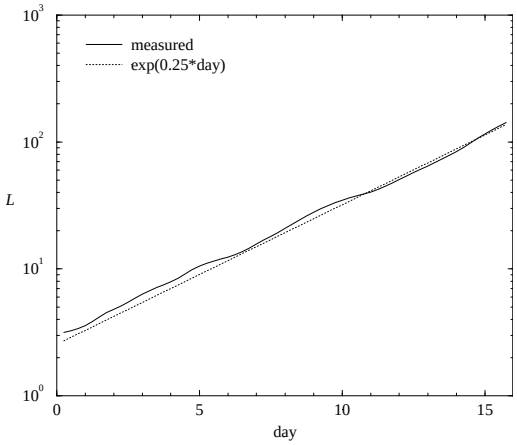

Figure 7: Growth of total length L of an interface in a stratospheric wind field. The overall interface grows exponentially, the dotted line is a fit to an exponential, although the majority of points only separate linearly with time, cf. figure 6. The interface length is given in multiples of the earth's radius $R_E = 6370\,\mathrm{km}$. See figure 2 for details of the advection process.

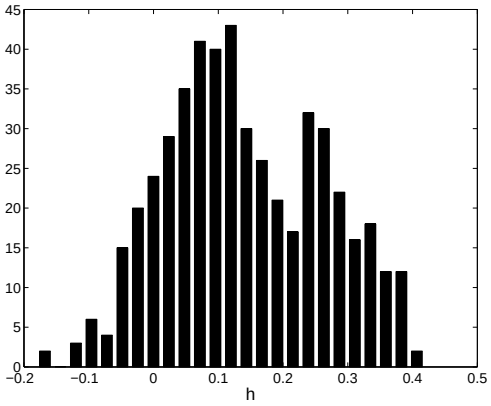

Figure 8: Histogram of finite time "Lyapunov exponents". The Lyapunov exponents are obtained by an exponential fit to the 500 particle pair separations used for figure 6. Note that the distances between tracer particle pairs are not rescaled during the advection process because the average maximal separation is only 0.25 rad (14°) which is not much larger than the distance of about 4° between the grid points where the wind field is defined.

using (27) (where E has been replaced by the mass of $ClONO_2$) and also the measured dimensions from figure 4. Integrating the rate of $ClONO_2$ production allows us to compare our results with the results of Tan et al. [20], see figure 9. We find that the total production of $ClONO_2$ increases about linearly with time which was also observed by Tan et al. For comparison, we have plotted the decay behaviour in the case of exponential interscale transfer. As expected, this case shows completely different behaviour for the production of $ClONO_2$. This is another indication that the interscale transfer of the flow is indeed linear and not exponential.

5 Conclusion

We have presented a new method to calculate the scalar variance dependence on the diffusivity from a snapshot of an on/off scalar field. Furthermore, we have shown that the method can be extended to mixing limited reactions of chemicals subject to advection. We have also predicted time dependent mixing for those cases where it is known that the flow has either linear or exponential interscale transfer. This new method is generally applicable to mixing and reaction processes of fractal and spiral chemical fields. We have studied one application of our method in detail: ClO deactivation in the lower stratosphere over the mid-northern latitudes. Not only have we recovered the diffusivity and time-dependence of chlorine deactivation, previously computed by Tan et al. [20], but we have furthermore extended their results for longer times and in particular for smaller more realistic diffusivities. In order to predict the time-dependence of chlorine deactivation, we have determined the interscale transfer of some stratospheric wind-fields. The results suggest that particle pairs separate on average linearly in the stratosphere (on a time scale of about 10 days) and consequently that the interscale transfer is dominantly linear.

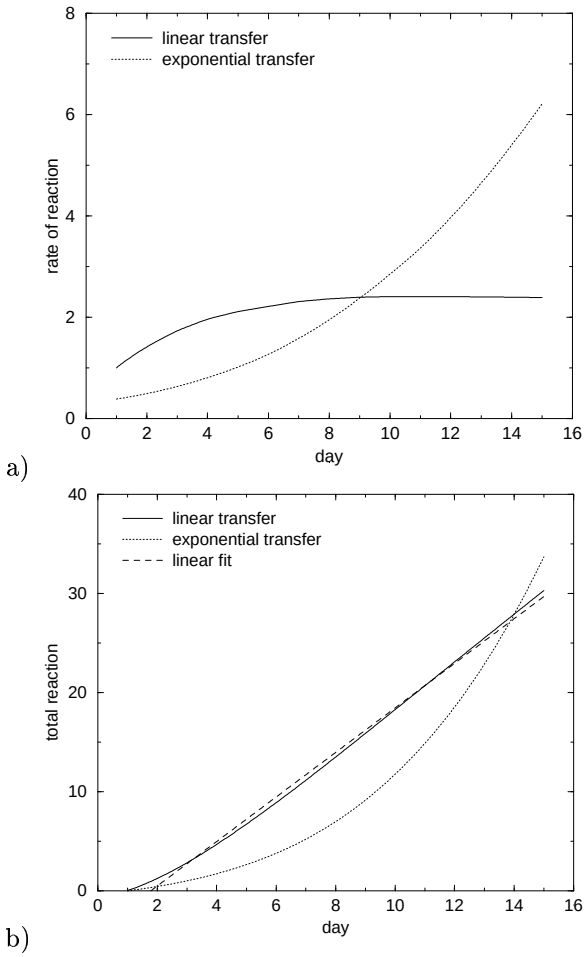

Figure 9: Predictions for time dependent mixing. The curves for linear interscale transfer are our predictions for the production of $ClONO_2$. The curves for exponential interscale transfer are drawn for comparison. a) Reaction rate calculated with Kolmogorov capacities as given in figure 4 and from (29) for linear interscale transfer and from (30) for exponential interscale transfer with a stretching rate of 0.25 d^{-1}, taken from figure 7. We observe that in the case of linear interscale transfer, the reaction rate becomes about constant after 5 days, whereas in the case of exponential interscale transfer the reaction rate continues to grow. b) Integration of curves in figure a) gives the total amount of reacted chemicals. We observe a linear like growth of the produced chemical in agreement with the results by Tan et al. [20].

This result challenges the conventional view that advection in the stratosphere is fully chaotic and suggests instead that there are only a few chaotic regions in the stratosphere which are separated by regions where the flow is of shearing nature.

Acknowledgements

We would like to thank the European Centre for Medium-Range Weather Forecasts for providing the raw wind data and Alan Iwi for processing the wind data for us. A.W. acknowledges the kind support of the Dr. Karl Wamsler Foundation and the NERC. J.C.V. gratefully acknowledges the support of the Royal Society.

References

[1] J.R. Angilella and J.C. Vassilicos. Spectral, diffusive and convective properties of fractal and spiral fields. *Physica D*, 124:23–57, 1998.

[2] J.R. Angilella and J.C. Vassilicos. Time-dependent geometry and energy distribution in a spiral vortex layer. *Phys. Rev. E*, 59:5427–5439, 1999.

[3] K.P. Bowman. Large-scale isentropic mixing properties of the antarctic polar vortex from analyzed winds. *J. Geophys. Res.*, 98:23013–23027, 1993.

[4] M.P. Chipperfield, E.R. Lutman, J.A. Kettleborough, and J.A. Pyle. Model studies of chlorine deactivation and formation of $ClONO_2$ collar in the arctic polar vortex. *J. Geophys. Res.*, 102(D1):1467–1478, 1997.

[5] S. Edouard, B. Legras, F. Lefèvre, and R. Eymard. The effect of small-scale inhomogeneities on ozone depletion in the arctic. *Nature*, 384:444–447, 1996.

[6] K.J. Falconer. *The geometry of fractal sets*. Cambridge University Press, 1985.

[7] D.R. Fereday, P.H. Haynes, A. Wonhas, and J.C. Vassilicos. Scalar variance decay in chaotic advection and batchelor-regime turbulence. *Phys. Rev. E (to be published)*, 2002.

[8] P. Flohr and J.C. Vassilicos. Accelerated scalar dissipation in a vortex. *J. Fluid Mech.*, 348:295, 1997.

[9] P. Haynes and J. Anglade. The vertical-scale cascade in atmospheric tracers due to large-scale differential advection. *J. Atmos. Sci.*, 54:1121–1136, 1997.

[10] M.N. Juckes and M.E. McIntyre. A high-resolution one-layer model of breaking planetary waves in the stratosphere. *Nature*, 328:590–596, 1987.

[11] F. Lefèvre, G.P. Brasseur, I. Folkins, A.K. Smith, and P. Simon. Chemistry of the 1991-1992 stratospheric winter: Three-dimensional model simulations. *J. Geophys. Res.*, 99(D4):8183–8195, 1994.

[12] J. Methven and B. Hoskins. The advection of high-resolution tracers by low-resolution winds. *J. Atmos. Sci.*, 56:3262–3285, 1999.

[13] L.T. Molina and M.J. Molina. Production of Cl_2O_3 from the self-reaction of the ClO radical. *J. Phys. Chem.*, 91:433–436, 1987.

[14] J.M. Ottino. *The kinematics of mixing: stretching, chaos, and transport.* Cambridge University Press, Cambridge, 1989.

[15] T. Peter. The stratospheric ozone layer – an overview. *Environmental Pollution*, 83:69–79, 1994.

[16] R.B. Pierce and T.D.A. Fairlie. Chaotic advection in the stratosphere: Implications for the dispersal of chemically perturbed air from the polar vortex. *J. Geophys. Res.*, 98(D10):18589–18595, 1993.

[17] R.T. Pierrehumbert and H. Yang. Global chaotic mixing on isentropic surfaces. *J. Atmos. Sci.*, 50:2462–2480, 1993.

[18] J.A. Pyle. Ozone loss in middle latitudes and the role of the arctic polar vortex. *Phil. Trans. R. Soc. Lond. A*, 352:241–245, 1995.

[19] S.J. Reid and G. Vaughan. Lamination in ozone profiles in the lower stratosphere. *Quart. J. R. Met. Soc.*, 117:825–844, 1991.

[20] D.G.H. Tan, P.H. Haynes, A.R. MacKenzie, and J.A. Pyle. The effects of fluid-dynamical stirring and mixing on the deactivation of stratospheric chlorine. *JGR-Atmospheres*, 103(D1):1585–1605, 1998.

[21] T. Tél, G. Károlyi, Á. Péntek, I. Scheuring, Z. Toroczkai, C. Grebogi, and J. Kadtke. Chaotic advection, diffusion and reactions in open flows. *Chaos*, 10:89–98, 2000.

[22] R. Toumi, R.L. Jones, and J.A. Pyle. Stratospheric ozone depletion by $ClONO_2$ photolysis. *Nature*, 365:37–39, 1993.

[23] A.F. Tuck and S.J. Hovde. Fractal behaviour of ozone, wind and temperature in the lower stratosphere. *Geophys. Res. Lett.*, 26:1271–1274, 1999.

[24] A.F. Tuck, S.J. Hovde, and M.H. Proffitt. Persistence in ozone scaling under the Hurst exponent as an indicator of the relative rates of chemistry and fluid mechanical mixing in the stratosphere. *J. Phys. Chem. A*, 103:10445–10450, 1999.

[25] A.F. Tuck et al. Polar stratospheric cloud processed air and potential vorticity in the northern hemisphere lower stratosphere at mid-latitudes during winter. *J. Geophys. Res.*, 97:7883–7904, 1992.

[26] J.C. Vassilicos. Anomalous diffusion of isolated flow singularities and of fractal or spiral structures. *Phys. Rev. E*, 52:R5753–R5756, 1995.

[27] J.C. Vassilicos and J.G. Brasseur. Self-similar spiral flow structure in low Reynolds number isotropic and decaying turbulence. *Phys. Rev. E*, 54:467–485, 1996.

[28] J.C. Vassilicos and J.C.R. Hunt. Fractal dimensions and spectra of interfaces with application to turbulence. *Proc. R. Soc. Lond. A*, 435:505–534, 1991.

[29] D.W. Waugh et al. Mixing of polar vortex air into middle latitudes as revealed by tracer-tracer scatterplots. *J. Geophys. Res*, 102(D11):13119–13134, 1997.

[30] C.R. Webster, R.D. May, D.W. Toohey, L.M. Avallone, J.G. Anderson, P. Newman, L. Lait, M.R. Schoeberl, J.W. Elkins, and K.R. Chan. Chlorine chemistry on polar stratospheric cloud particles in the arctic winter. *Science*, 261:1130–1134, 1993.

[31] WMO. Scientific assessment of ozone depletion: 1994. *WMO Ozone Res. Monitoring Proj. Rep. No. 37*, 1995.

[32] A. Wonhas and J.C. Vassilicos. Mixing in frozen and time-periodic two-dimensional vortical flows. *J. Fluid Mech.*, 442:359–385, 2001.

[33] A. Wonhas and J.C. Vassilicos. Mixing in fully chaotic flows. *Phys. Rev. E* (submitted, 2001).